Article

Low-Cost and Recyclable Photocatalysts: Metal Oxide/Polymer Composites Applied in the Catalytic Breakdown of Dyes

Timur Borjigin [1,2], Michael Schmitt [1,2,*], Fabrice Morlet-Savary [1,2,*], Pu Xiao [3,*] and Jacques Lalevée [1,2,*]

1 Université de Haute-Alsace, CNRS, IS2M UMR 7361, F-68100 Mulhouse, France
2 Université de Strasbourg, 67000 Strasbourg, France
3 Research School of Chemistry, Australian National University, Canberra, ACT 2601, Australia
* Correspondence: michael.schmitt@uha.fr (M.S.); fabrice.morlet-savary@uha.fr (F.M.-S.); pu.xiao@anu.edu.au (P.X.); jacques.lalevee@uha.fr (J.L.)

Abstract: Novel metal oxide/polymer composite photocatalysts prepared by photocuring with common metal oxide particles (ZnO or CeO_2) and acrylic ester monomers have been investigated for the first time. Metal oxide particles were fully integrated with the acrylate polymer network based on the crosslink of poly ethylene glycol diacrylate (noted below as Poly-PEG) by photopolymerization upon mild light source (LED@405 nm) irradiation. The prepared metal/oxide composite showed excellent performance in the photodegradation of Acid Black dye (used as a benchmark pollutant) in an aqueous environment. Indeed, under UV lamp irradiation for 60 min, the degradation of Acid Black reached 59% and 56%, in the presence of 10 wt% ZnO/Poly-PEG and 3 wt% CeO_2/poly PEG, respectively. Markedly, the new reported photocatalysts have offered much better performance over the conventional TiO_2 photocatalytic material used as a control (39% degradation using 1 wt% TiO_2/poly PEG). In turn, the new proposed metal oxide/polymer composites were further characterized by a range of analytical characterization methods, including the swelling test, thermogravimetric analysis (TGA), scanning electron microscopy (SEM), X-ray diffraction analysis (XRD), dynamic mechanical analysis (DMA), UV–visible diffuse reflectance spectroscopy, and electron spin resonance analysis. The results showed that the new photocatalysts demonstrated excellent water adsorption properties, high-temperature resistance, and excellent recyclability, which were very suitable for wide application and in line with the concept of green chemistry.

Keywords: metal oxide/polymer composites; photopolymerization; photocatalyst; dye degradation

1. Introduction

Due to the pollution of surface water and groundwater in many countries, water pollution control has received widespread attention worldwide [1]. Pollutants in water come from many industrial fields such as oil refining, chemicals, steel, coal, paper, textiles, etc. In addition, herbicides, pesticides, fertilizers, and transportation fuels used in agriculture are also sources of pollution that cannot be ignored [2]. Current wastewater treatment technologies are basically separation processes, such as sedimentation, flocculation, filtration, adsorption, gas extraction, etc. [3,4]. These processes have the advantage of being mature and easy to apply on a large industrial scale. However, there are still some issues with these technologies such as low efficiency, being prone to secondary pollution or narrow scope of use, only for specific pollutants or high energy consumption, not suitable for large-scale dissemination, and other defects [5–7]. Therefore, the development of chemical pollutant removal technologies with high efficiency, low energy consumption, wide applicability, and deep oxidation capability has been the goal of environmental technology.

As the research progresses, it has been found that the semiconductor photocatalytic oxidation technology demonstrates the outstanding advantages of low energy consumption, strong oxidation capacity, mild reaction conditions, easy operation, and reduction of

secondary pollution in the removal of pollutants, and has attractive application prospects and may gradually become a practical industrial technology [8,9]. Many experiments have proved that dyes [10–12], surfactants [13], organohalides [14], pesticides [15], cyanides [16], phenols [17], PCBs [18], and PAHs [19] can be effectively degraded, decolorized, and detoxified by photocatalytic oxidation, and finally mineralized into inorganic small molecules, thus eliminating or slowing down the pollution to the environment. Photocatalytic oxidation, one of the advanced oxidation technologies, is a technology that uses photogenerated strong oxidants to completely oxidize organic pollutants into small molecules such as water, carbon dioxide, etc. This method can treat a variety of pollutants, has a wide range of applications, especially for the difficultly degradable organic matter with good oxidation and decomposition, and has the advantage of using sunlight as the reaction light source, and is a very promising pollution treatment which has received a lot of attention in recent years [20,21].

Zinc oxide (ZnO) is an important semiconductor material with similar bandwidth as the common photocatalyst TiO_2, and it has the advantages of simple preparation and low price [22–24]. Therefore, the use of ZnO as a photocatalyst for the photocatalytic degradation of organic pollutants has attracted increasing attention [25,26]. However, due to the wide band gap of ZnO nanoparticles, the excitation of electrons in the valence band to the conduction band requires high energy, and the photocatalytic effect can be achieved only under the irradiation of UV light [27,28]. In practical applications, the cost of UV light sources is high, and the proportion of UV light in sunlight is only about 5%, which is much lower than the proportion of visible light, thus greatly limiting its practical applications [29]. A polymer compounded with nanoparticles can play the role of particle refinement, and the particle size is reduced, so that the photogenerated electrons and holes can be easily trapped on the particle surface, thus reducing the chance of electron–hole complexation, and improving the photocatalytic efficiency. At the same time, the electrons in the conjugated polymers have a high degree of delocalization and a relatively small energy gap, which can absorb light from UV to IR [30,31]. When the inorganic semiconductor is compounded with the conjugated polymer, under the irradiation of natural light, electrons can be transferred from the polymer to the conduction band of the inorganic nanoparticles, and the electrons in the valence band of the inorganic nanoparticles can be transferred to the conjugated polymer, which reduces the chance of electron–hole complexation and broadens the spectral response range of the whole system due to the presence of the conjugated polymer, thus greatly improving the photocatalytic performance [32,33].

In addition, cerium dioxide (CeO_2) is an extremely versatile rare earth oxide and a light yellow powder with n-type semiconductor properties, rich energy levels, special electron orbital structure, unique optical properties, strong adsorption selectivity, good thermal stability, electrical conductivity, etc. [34–36]. Ce(IV) ions are arranged in the face center and at the vertices of the cubic structure, and $O(^{2-})$ ions are simply embedded in the cubic structure [37]. CeO_2 is converted to non-chemometric CeO_{2-x} after reduction at temperatures above 900 °C, at which point it loses a significant amount of oxygen in the lattice and forms an oxygen deficiency [38]. This shows that CeO_2 has a good ability to store and release oxygen and can be widely used in the field of catalysis. However, CeO_{2-x} retains its fluorite-type crystal structure and can be reconverted to CeO_2 when exposed to oxidizing environments [39]. CeO_2 can effectively degrade organic pollutants under light irradiation. For example, it has been reported that the band gap of CeO_2 can be modulated by electron beam irradiation and the modulated CeO_2 exhibited better photocatalytic activity for the degradation of 4-nitrophenol and methylene blue under visible light irradiation [40]. The photocatalytic activity was found to be better for the degradation of 4-nitrophenol and methylene blue under visible irradiation. Moreover, it has been reported that CeO_2 nanotubes can be used to photo-degenerate the health-harmful Cr(VI) to the less toxic and more easily precipitated Cr(III) [41]. In contrast, the application of composites composed of CeO_2 and polymers for pollutant degradation has been rarely reported [42].

Herein, to the best of our knowledge, two low-cost, environmentally friendly, and green chemistry compliant metal oxide/polymer composites with high photocatalytic properties were synthesized for the first time by the photopolymerization approach under a mild and low-cost LED irradiation source. The composite obtained by photopolymerization retains the photocatalytic properties of the metal oxides while the stability of the cross-linked polymer and the good bonding of the metal oxide particles to the polymer makes the metal oxide powder easier to recover after using the material for the photodegradation of water pollutants. This approach strongly simplifies the carrier design process for photocatalysts such as ZnO, TiO$_2$, and CeO$_2$, and greatly reduces the cost of pollution treatment.

Metal oxides, polymers, and degraded dyes are common in industrial production. The metal oxides were originally inserted by photopolymerization in an acrylate polymer network based on the crosslink of poly ethylene glycol diacrylate (noted below as Poly-PEG). The new proposed metal oxide/polymer composite photocatalysts showed excellent photocatalytic ability when facing the problem of water pollution caused by Acid Black and Eosin-Y under UV lamp irradiation. Meanwhile, the mechanism of the photocatalytic process was explained and summarized to some extent after a series of analytical tests by characterization techniques such as thermogravimetric analysis, scanning electron microscopy, X-ray diffraction analysis, dynamic mechanical analysis, UV–Vis diffuse reflectance spectroscopy, and electron spin resonance analysis. Current research on the modification of metal oxide photocatalysts is mainly focused on compliance with other semiconductor materials, while compounding with polymers is less common. Therefore, the study of polymer modification of common metal oxide photocatalysts by physical and chemical means in the absence of co-catalysts is full of positive implications.

2. Materials and Methods

2.1. Chemical Compounds Used in This Work

Poly ethylene glycol (600) diacrylate (PEGDA) and trimethylolpropane triacrylate (TMPTA) were selected as monomers for composite synthesis and were purchased from Allnex. 2-Benzyl-2-dimethylamino-1-(4-morpholinophenyl)-butanone-1 (Speedcure BDMB) was obtained from Lambson Ltd. (Wetherby, UK) and used as the photoinitiator. Acid Black and Eosin-Y were purchased from Sigma-Aldrich. Chemical structures of the reagents used in this study are shown in Scheme 1. The metal oxides used were zinc oxide (ZnO), 99.99% (metals basis) from Thermo Fisher Scientific (87812) and cerium(IV) oxide (CeO$_2$) was obtained from Solvay. Titanium(IV) oxide (TiO$_2$), anatase, 99.8% (metals basis) was from Sigma-Aldrich (232033).
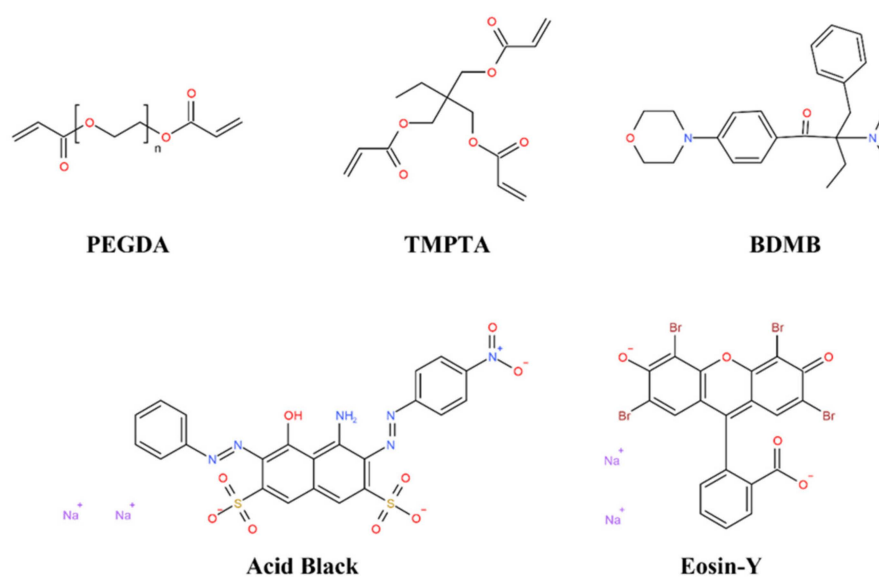
Scheme 1. Chemical structures of the compounds.

2.2. Photopolymerization Experiments

First, the different proportions of metal oxide particles, BDMB and PEGDA or TMPTA, were mixed at high speed (2500 rpm, 3 min) and the resulting slurry was immediately placed in a small, fixed mold (8 mm diameter and 4 mm height/thickness) for the photocuring process upon light exposure (light resource: light emitting diode (LED)@405 nm, I_0 = 110 mW·cm^{-2}). The obtained formulations were also deposited in laminate between two polypropylene films for researching evolution of the double bond content of acrylates during the polymerization reaction. Particularly, 1 or 2 drops are enough to control the thickness at ~100 µm, then the formulations were exposed to LED@405 nm (I_0 = 110 mW·cm^{-2}) to initiate the free radical polymerization (FRP) at room temperature and. During the polymerization processes, the IR peak at ~6120 cm^{-1}, corresponding to a characteristic peak of the PEGDA or TMPTA, was continuously monitored by real-time FTIR spectroscopy (JASCO FTIR 4100). The experimental set-up was used in previous work [22]. The polymerization profiles were established using the following relationship of acrylate function conversion at a given irradiation time (where A_0 is the initial peak area before irradiation and A_t is the peak area after irradiation for a given time t):

$$\text{Conversion}(\%) = \frac{A_o - A_t}{A_o} \times 100. \tag{1}$$

2.3. Photocatalytic Experiments

The photodegradation of Acid Black took place under the irradiation of UV lamps in water solution, whose concentration was 15 ppm (24.25 µmol·L^{-1}, pH = 5.9). First, 4 mL of the above solution was added to the cuvette together with the prepared metal oxide/polymer composite photocatalyst. After every 15 min of irradiation, the cuvette was placed in a JASCO V730 spectrophotometer for UV–Vis absorption spectroscopy and the change in the absorption peak at 618 nm (maximum absorption wavelength of Acid Black solution) was observed.

The discoloration of the dye at different irradiation times was calculated by the following formula:

$$\text{Conversion}(\%) = \frac{\text{Abs}_{to} - \text{Abs}_t}{\text{Abs}_{to}} \times 100 \tag{2}$$

where Abs_{t0} and Abs_t are the measured dye absorbances before and after a given time (t) of irradiation by an Omnicure Dynamic UV lamp, series 1000 lumen (I_0 = 250 mW·cm^{-2}, λ = 320–520 nm).

2.4. Composite Stability in Aqueous Phase

Swelling experiments were carried out by impregnating composites and polymer in water for 12 h. The dry extracts of the composites were calculated after the swelling experiments by drying them in an oven at 50 °C for 1 h. The swelling ratio and the dry extract were calculated using the following formula:

$$\text{Swelling ratio}(\%) = \left(\frac{m_w}{m_0} - 1 \right) \times 100, \tag{3}$$

$$\text{Dry extract}(\%) = \frac{m_l}{m_0} \times 100, \tag{4}$$

where m_0 is the initial weight of polymer or composite, m_w is the weight of swollen polymer or composite, and m_l is the weight of dried polymer or composite.

2.5. Thermal Stability

The thermogravimetric analysis (TGA) was realized using a TGA Mettler Toledo TGA/DSC3+. The experiments were carried out at temperatures ranging from 30 °C to 800 °C at a heating rate of 10 K/min under a dry airflow of 100 mL/min.

2.6. SEM Characterization

A JSM-7900F scanning electron microscope (SEM) from JEOL was used in this study.

2.7. XRD Characterization

X-ray diffraction patterns were recorded using a Panalytical X'Pert PRO diffractometer equipped with a Cu X-ray tube (CuKα = 0.1542 nm) operating at 45 kV and 40 mA, and a PIXCel detector. The full width at half maximum (FWHM) was determined using pseudo-Voigt functions for XRD analysis, as described in the publication of Schmitt [23].

2.8. Mechanical Properties

Dynamic mechanical analysis (DMA) was measured using DMA Mettler Toledo DMA861e. Dynamic storage modulus G of different composites was evaluated to determine their mechanical properties.

2.9. Optical Properties

UV–visible diffuse reflectance spectra measurements were performed using a UV–visible spectrophotometer (JASCO V-750) equipped with an integrating sphere.

### 2.10. Electron Spin Resonance (ESR Experiments)

ESR-ST experiments were carried out using an X-band spectrometer (Bruker EMX-plus). An LED@405 nm was used as the irradiation source at room temperature under air. The free radicals generated were trapped by phenyl-N-tert-butylnitrone (PBN). The ESR procedure has been described in the literature for other photocatalysts [11,12].

3. Results and Discussion

3.1. Synthesis of Metal Oxide/Polymer Composites by Photopolymerization

By high-speed mixing, the different ratios of ZnO or CeO_2 powders were dispersed in PEGDA monomers (average mass 610 g/mol). The sample of 1 wt% TiO_2/Poly-PEG was also prepared as a benchmark composite for the photodegradation experiment. The photopolymerization of materials consisting of metal oxides fillers and monomers was initiated by the photoinitiator BDMB (0.2 wt%). Under the irradiation of an LED light source, the photoinitiated free radical polymerization (FRP) proceeded rapidly and achieved a very high conversion level. The photopolymerizations of the free radical polymerization of PEGDA in laminate upon exposure to LED@405 nm were investigated using real-time FTIR and are shown in Figure 1.

Figure 1a shows the polymerization of the resin under mild LED (405 nm) irradiation with different weight contents of ZnO. It demonstrated that the addition of ZnO influenced the conversion rate of PEGDA. Specifically, a decrease in the polymerization properties of the resin occurred as the proportion of ZnO filler increased, which can be ascribed to the scattering and absorption of light and the blocking of light penetration by the fillers. If the content increased to 10 wt%, the conversion of the resin decreased by about 5%. However, this negative effect was not so obvious with a low incorporation of ZnO. Similarly, the addition of CeO_2 had a more sensitive response to the polymerization of PEGDA at low levels compared to ZnO (Figure 1b). However, when the content increased to 10%, the decrease in polymerization conversion was similar to the 10% ZnO/polymer composite.
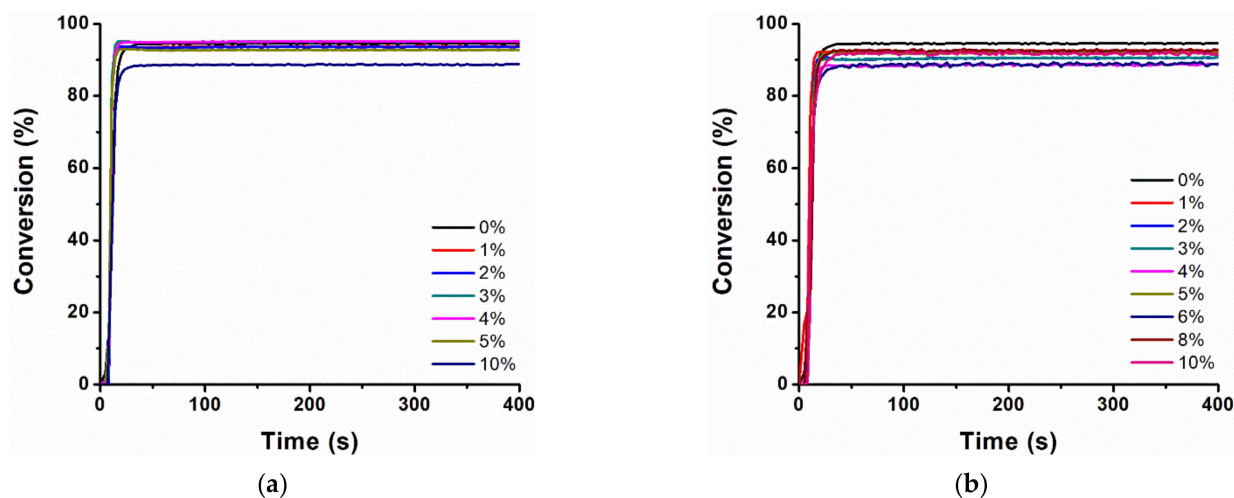
Figure 1. Photopolymerization profiles of acrylate functions (double bond conversion vs. irradiation time) in laminate upon exposure to LED@405 nm (**a**) in the presence of BDMB (0.2 wt%)/ZnO (0~10 wt%); (**b**) in the presence of BDMB (0.2 wt%)/CeO$_2$ (0~10 wt%); thickness at ~100 μm; the irradiation starts at t = 10 s.

In order to visualize the effect of the addition of metal oxide powder on the depth of cure (DoC) characterizing the polymerization performance of the photocurable resin, the resin mixed with different contents of fillers was injected into a circular container (50 mm diameter) and subjected to photopolymerization reaction for 2 min under the irradiation of LED@405 nm (1 W·cm^{-2}). Finally, the cured samples were removed, and their thicknesses were measured separately. The results are shown in Figure 2, in which a significant correlation of the filler content with the thickness of the sample is observed. Specifically, the higher filler content resulted in the thinner thickness of the prepared metal oxide/polymer composites. Again, the light penetration issue for filled samples reduced the DoC but, interestingly, thick coatings (1–2 mm) can even be prepared with 10% weight of catalyst.
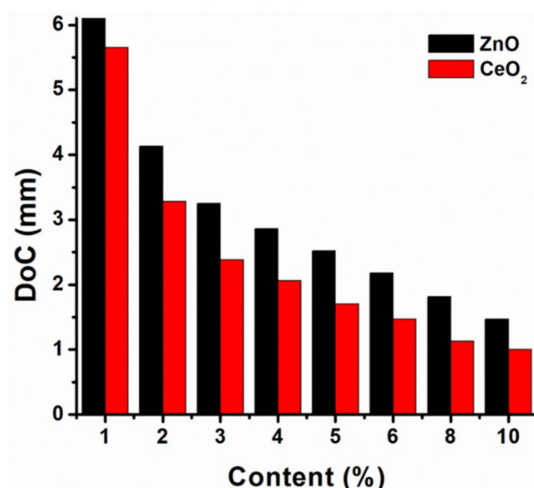
Figure 2. Depth of cure (DoC) of the samples synthesized using different wt% of metal oxides and PEGDA in the presence of 0.2 wt% BDMB under air upon exposure to LED@405 nm.

3.2. Metal Oxide/Polymer Composite Stability

In industrial applications, the stability and recyclability of the photocatalyst is a decisive factor for large-scale production and application. Therefore, it is necessary to study the stability of photocatalysts under different application environments.

3.2.1. Stability in Aqueous Phase

In the application of photocatalyst for wastewater treatment, the adsorption properties and stability of photocatalyst immersed in water are of particular importance. Therefore, to investigate metal oxide/polymer composites stabilities, swelling experiments were carried out in aqueous phase solvent.

It is obvious from Figure 3 that after 12 h of exposure to water, both the Poly-PEG and metal oxide/Poly-PEG showed a high swelling rate, which reflected their excellent water absorption properties. It also represented a larger specific surface area of the photocatalyst in contact with the solution, which was beneficial for the adequate reaction of the photocatalyst with the dye. At the same time, the addition of fillers demonstrated the limited effect on the water absorption properties of the composites. It also indicated that ZnO and CeO_2 were very well integrated in the internal structure of the polymers.
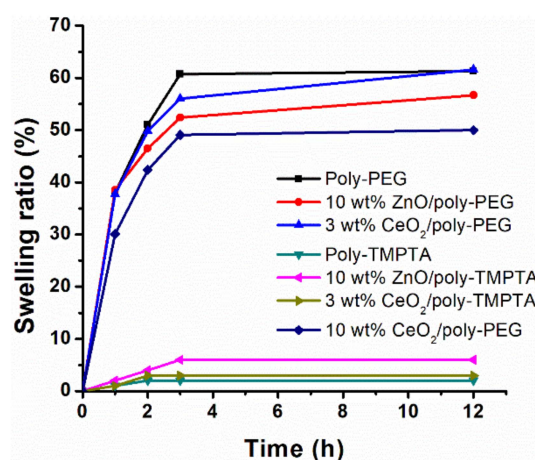
Figure 3. Swelling of different samples after water absorption, in terms of swelling ratio before and after water absorption (%).

In contrast, if the monomer was replaced with TMPTA, no significant swelling occurred when the samples were immersed in water even for a long time (more than 12 h). Compared to Poly-PEG and metal oxide Poly-PEG, the water absorption properties of Poly-TMPTA and metal oxide Poly-TMPTA were obviously extremely low, which also greatly affected the performance of their application in dye photodegradation.

Dry extracts (%) for the different synthesized metal oxide/polymer composites were also analyzed and are presented in Table 1 to evaluate the monomer/filler loss probability of the composite after immersion in water. After water absorption and swelling, the drying process was carried out for one hour in the oven (50 °C) for different samples. It was obvious that the drying process did not lead to significant large mass loss compared to the original sample, which facilitated the recycling of the samples. Therefore, in the design of photocatalysts, PEGDA illustrated more significant advantages than TMPTA for the application.

Table 1. Dry extract (%) for the different synthesized metal oxide/polymer composites measured after drying the swollen samples for one hour in the oven (50 °C).

Composites	Dry Extract (%)
Poly-PEG	100 ± 2
10 wt% ZnO/Poly-PEG	98 ± 2
3 wt% CeO_2/Poly-PEG	100 ± 2
Poly-TMPTA	100 ± 2
10 wt% ZnO/Poly-TMPTA	100 ± 2
3 wt% CeO_2/Poly-TMPTA	100 ± 2
10 wt% CeO_2/Poly-PEG	95 ± 2

3.2.2. Thermal Stability

To evaluate the thermal stabilities of polymers and metal oxide/polymer composites, thermogravimetric (TG) analyses were performed. Decomposition temperatures of the different synthesized materials are shown in Figure 4.
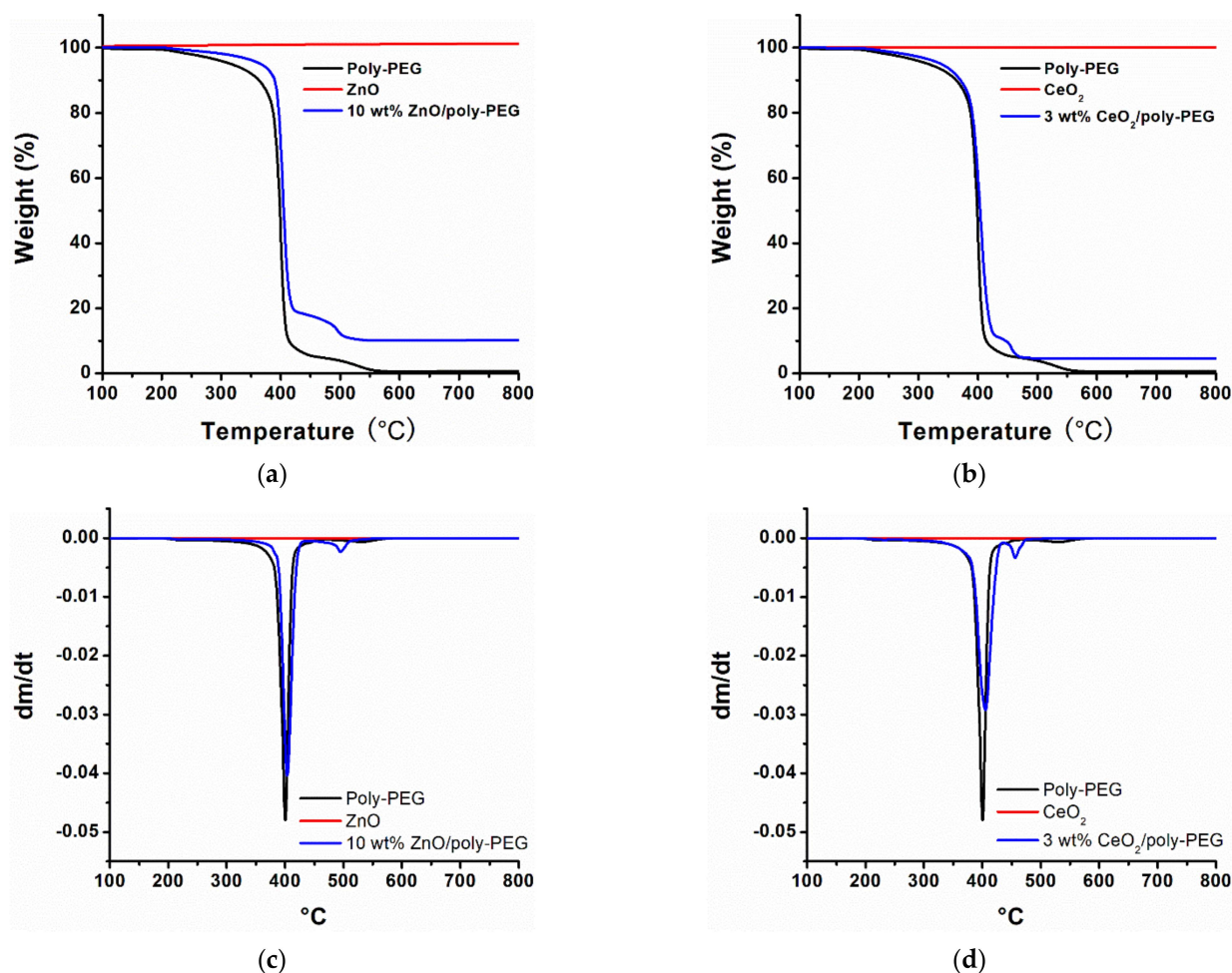
Figure 4. Decomposition temperatures of (**a**) Poly-PEG, ZnO powder, and 10 wt% ZnO/Poly-PEG composite; (**b**) Poly-PEG, CeO_2 powder, and 3 wt% CeO_2/Poly-PEG composite. TGA curves of (**c**) Poly-PEG, ZnO powder, and 10 wt% ZnO/Poly-PEG composite; (**d**) Poly-PEG, CeO_2 powder, and 3 wt% CeO_2/Poly-PEG composite.

From the results of TGA experiments, the thermal decomposition temperature of Poly-PEG is about 400 °C, while both ZnO and CeO_2 showed extremely high thermal stability at this temperature and even higher temperatures. The newly synthesized ZnO/Poly-PEG and CeO_2/Poly-PEG composites demonstrated similar thermal decomposition temperatures to Poly-PEG. This performance made the new photocatalysts highly dependable for applications at high temperatures.

3.3. Metal Oxide/Polymer Composite Characterization

To verify the metal oxide powder immobilization in the polymer, additional morphological and structural characterizations of the developed composites were carried out considering that the photocatalysis processes usually occur at the photocatalyst interface for heterogenous photocatalysis. Furthermore, for practical applications, it was also important to investigate their optical and mechanical properties.

3.3.1. Morphological Characterizations

The developed metal oxide/polymer composite morphologies were characterized using scanning electron microscopy (SEM). Selected images are shown in Figure 5. To better observe the intrinsic morphological and structural changes before and after compounding, both surface and cross-section SEM images of the samples were measured. The subsequent photopolymerization step allowed these metal oxide particles to be anchored in the framework of the polymers.
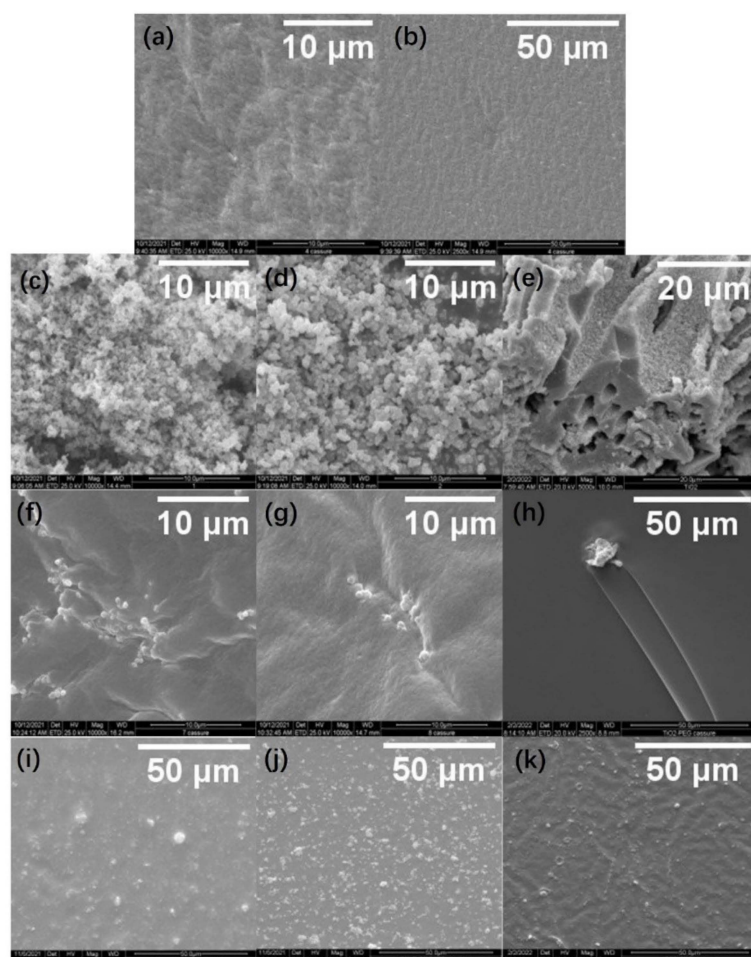

Figure 5. SEM images of (**a**) cross-section of Poly-PEG, (**b**) surface of Poly-PEG; (**c,d,e**) ZnO, CeO$_2$, and TiO$_2$ powder; (**f–h**) cross-section of 10 wt% ZnO/Poly-PEG, 3 wt% CeO$_2$/Poly-PEG, and 1 wt% TiO$_2$/Poly-PEG; (**i–k**) surface of 10 wt% ZnO/Poly-PEG, 3 wt% CeO$_2$/Poly-PEG, and 1 wt% TiO$_2$/Poly-PEG.

The SEM images of ZnO and CeO$_2$ show that the metal oxides were mostly uniform in size. The particle size was basically in the nanometer range. The surface and cross-section of TMPTA and PEGDA samples were smoother and tightly structured. When different contents of ZnO and CeO$_2$ were doped into the polymers, the appearance of metal oxide particles was clearly visible in SEM images, uniform and independent, both in TMPTA- and PEGDA-based samples. The addition of these particles did not significantly damage the intrinsic structure of the polymers, but rather formed a composite structure with the polymers relatively well distributed. Given the excellent adsorption properties of the metal oxide/Poly-PEG composite mentioned earlier, the pollutants can be more fully and efficiently in contact with the metal oxides for photocatalytic reactions. It is noteworthy that by visual comparison, ZnO exhibited better dispersion in Poly-PEG than in Poly-TMPTA.

3.3.2. X-Ray Diffraction (XRD)

The XRD patterns of the synthesized Poly-PEG, 10 wt% ZnO/Poly-PEG composite, and 3 wt% CeO_2/Poly-PEG composite are shown in Figure 6. As can be seen, the diffraction peaks of all composites corresponded clearly to the standard PDF cards (ZnO:01-070-8070; CeO_2: 00-067-0121), which meant that, during the process of photopolymerization, no other side products were generated. The crystallite size for ZnO is in the range of 79 ± 3 nm. No significant difference is observed if the particles are dispersed in the polymer matrix. For CeO_2, a crystallite size of 70 ± 5 nm could be calculated. The fabrication of metal oxide/polymer composites was successful.

(a)

(b)

(c)
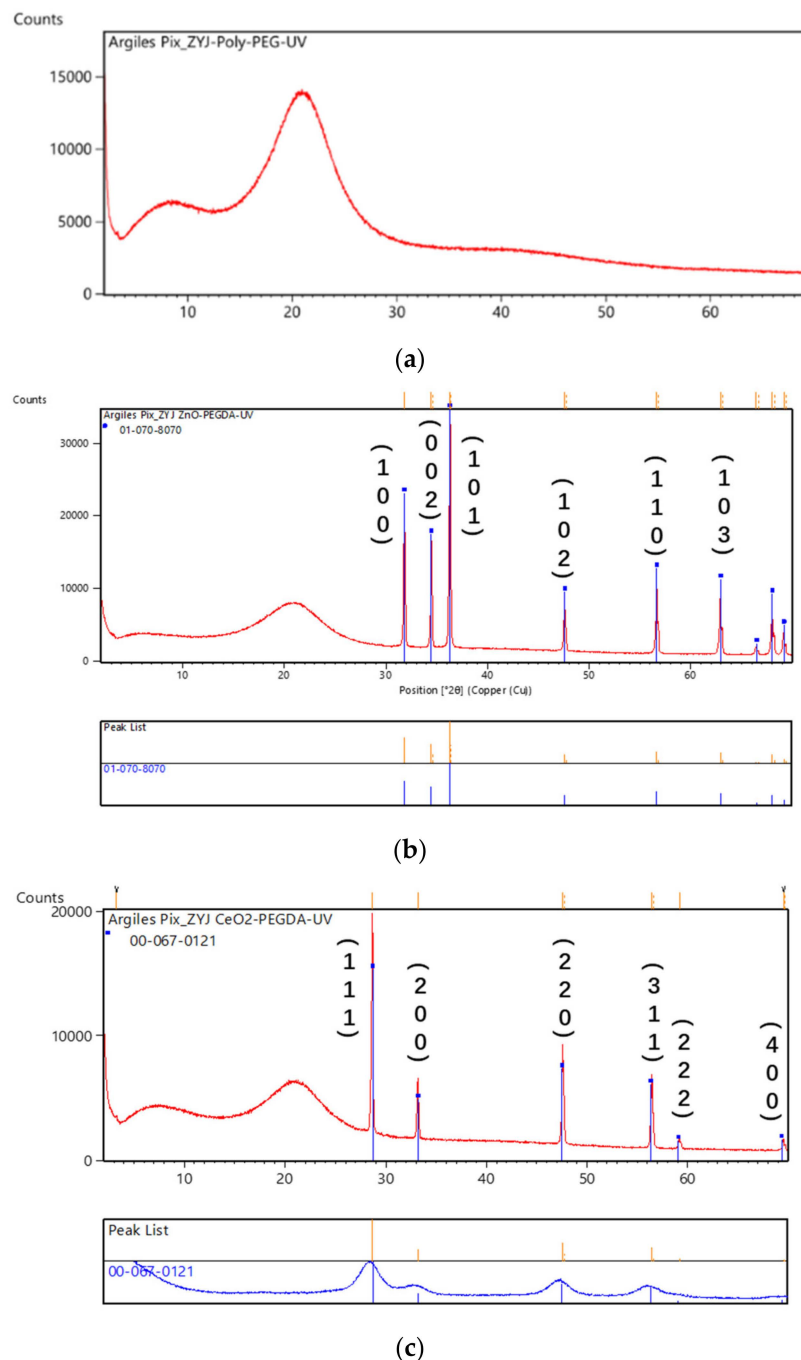
Figure 6. XRD analysis of (**a**) Poly-PEG, (**b**) 10 wt% ZnO/Poly-PEG composite, and (**c**) 3 wt% CeO_2/Poly-PEG composite.

3.3.3. Mechanical Properties

Mechanical properties of the synthesized composites were investigated using dynamic mechanical analysis (DMA). The obtained values of dynamic storage modulus G′ at room temperature (25 °C) are presented in Figure 7.
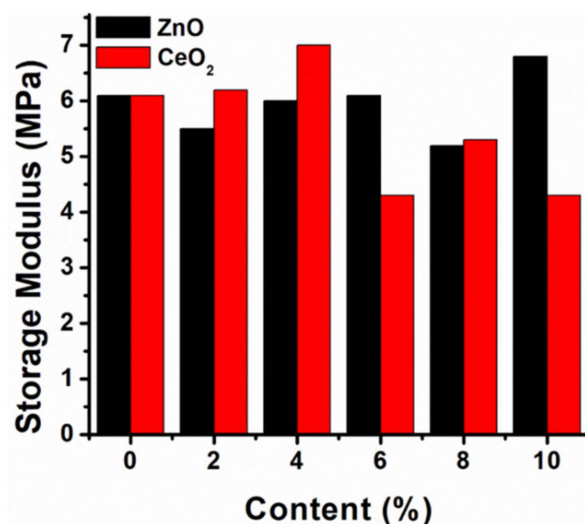

Figure 7. Dynamic storage modulus (G′) at 25 °C of metal oxide/Poly-PEG with different metal oxide mass ratios.

For the samples without any metal oxide particles, the G′ value of the Poly-PEG substrate was about 6.1 MPa. The highest G′ values can be attained if the ZnO content is 10% while the CeO_2 content is 4%. However, it was interesting that the G′ values of the composites did not change significantly as the amount of metal oxide particles mixed into the substrate gradually increased, with a fluctuation interval of only about plus or minus 1 MPa. In other words, for the investigated composites, the mixing of the metal oxide particles did not alter the mechanical properties. This can be microscopically seen in the intrinsic matrix structure of the polymers which was not disrupted by the compounding behavior.

3.3.4. Optical Properties

Among the many factors influencing the photocatalytic processes, the light absorption ability of the catalyst is important. Therefore, the optical properties of new composites were studied using UV–visible diffuse reflectance spectra and the results are shown in Figure 8.

The light reflection peaks of the composites generated a red-shift in the emission range of the 405 nm LED with the increase in the metal oxide particle content, which was especially obvious for CeO_2/Poly-PEG. This indicated an increase in the range of light absorption by the composites. The results of apparent absorbance limits are listed in Table S1. The light absorption wavelength interval of the composites matched with the optical properties of ZnO and CeO_2 particles reported in the relevant literature [28,42]. Taking into account that the XRD data do not change after the formation of the composites, the polymer, which was used as a substrate, also does not affect the light absorption properties of the metal oxide, but served as protection. The accurate and intense absorption of light in the UV wavelength range was an advantage for the photocatalytic performance of these new composites.
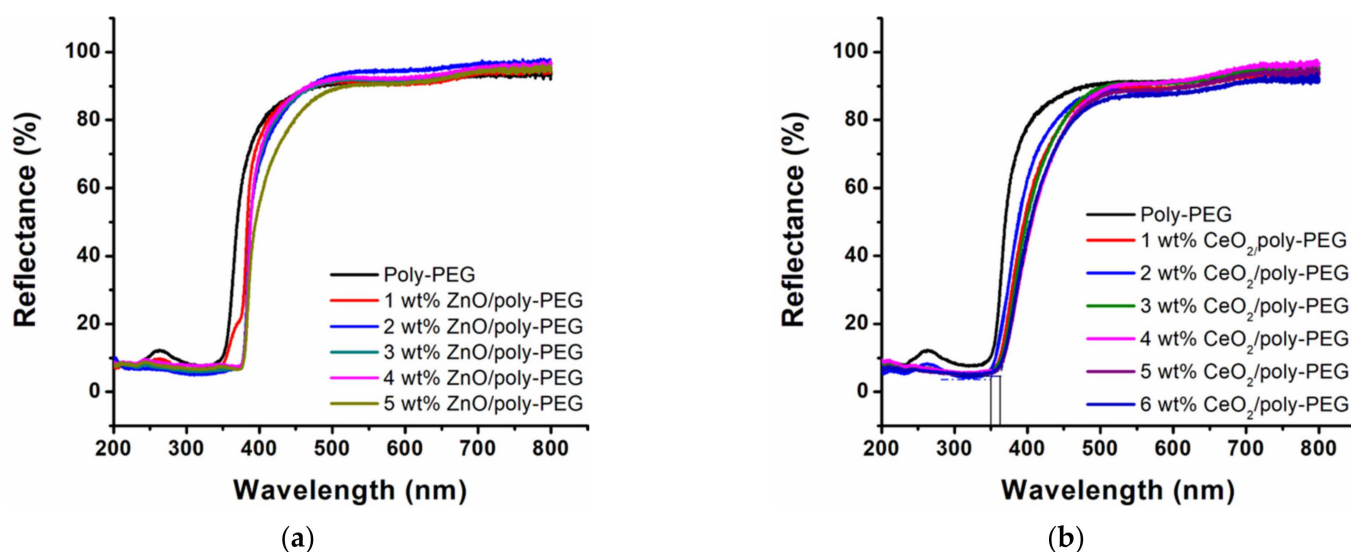
Figure 8. UV–visible diffuse reflectance spectra of (**a**) Poly-PEG and ZnO/Poly-PEG; (**b**) Poly-PEG and CeO_2/Poly-PEG.

3.4. Photocatalytic Activity of the Metal Oxide/Polymer Composites

As a photocatalytic test, the degradation of Acid Black and Eosin-Y in aqueous solution under UV lamp irradiation was carried out on the synthesized metal oxide/polymer composites. According to the literature [12], Acid Black exhibits two distinct absorption bands. The maximum absorption is at 618 nm, which corresponds to the azo group (N=N). The second absorbance between 200 and 400 nm corresponds to electron vibration transitions in benzene and naphthalene substructures (see Figure 9a–c), in the aromatic part. A decrease in absorbance during the photocatalytic treatment indicated degradation of the dye aromatic part. For an intuitive understanding of the photocatalytic properties of the new composites, 1 wt% TiO_2/Poly-PEG was applied in the investigation as a benchmark.

Figure 9a–c show the effectiveness of metal oxide/polymer composites for the Acid Black photodegradation. Without irradiation (in dark conditions), there is no significant degradation of the dye (<5%). This clearly shows that a photochemical process is associated with the degradation. The absorption maxima at 618 nm steadily diminished during the irradiation, showing the breakdown of the azo N=N bond and the naphthalene groups. For ZnO/Poly-PEG (Figure 9d), the photodegradation of Acid Black by the new photocatalyst was positively correlated with the increase in ZnO content. The increase in photocatalytic capability reached a plateau at around 59% for 10 wt% of ZnO (Figure 9d). Thereafter, the effect of enhancing the photocatalyst performance by means of increasing the ZnO content was not obvious. Interestingly, the results of CeO_2/Poly-PEG had a different performance (Figure 9e). Specifically, the increase in CeO_2 also improved the catalytic performance significantly at the mixed content of 0–3%. The catalyst with a CeO_2 content of 3% demonstrated the best catalytic performance (Acid Black degeneration ~56%). However, when the content was higher than 3%, the continued addition of CeO_2 caused a marked decrease in the catalytic performance. At a CeO_2 content of 6%, the performance was even almost equal to that of the polymer matrix without CeO_2. It may be attributed to the fact that the increased amount of CeO_2 may not be better wetted by the PEGDA. Accordingly, ZnO and CeO_2 in the new composite are required to have an optimum content (10 wt% and 3 wt%, respectively) to achieve the best catalytic performance.
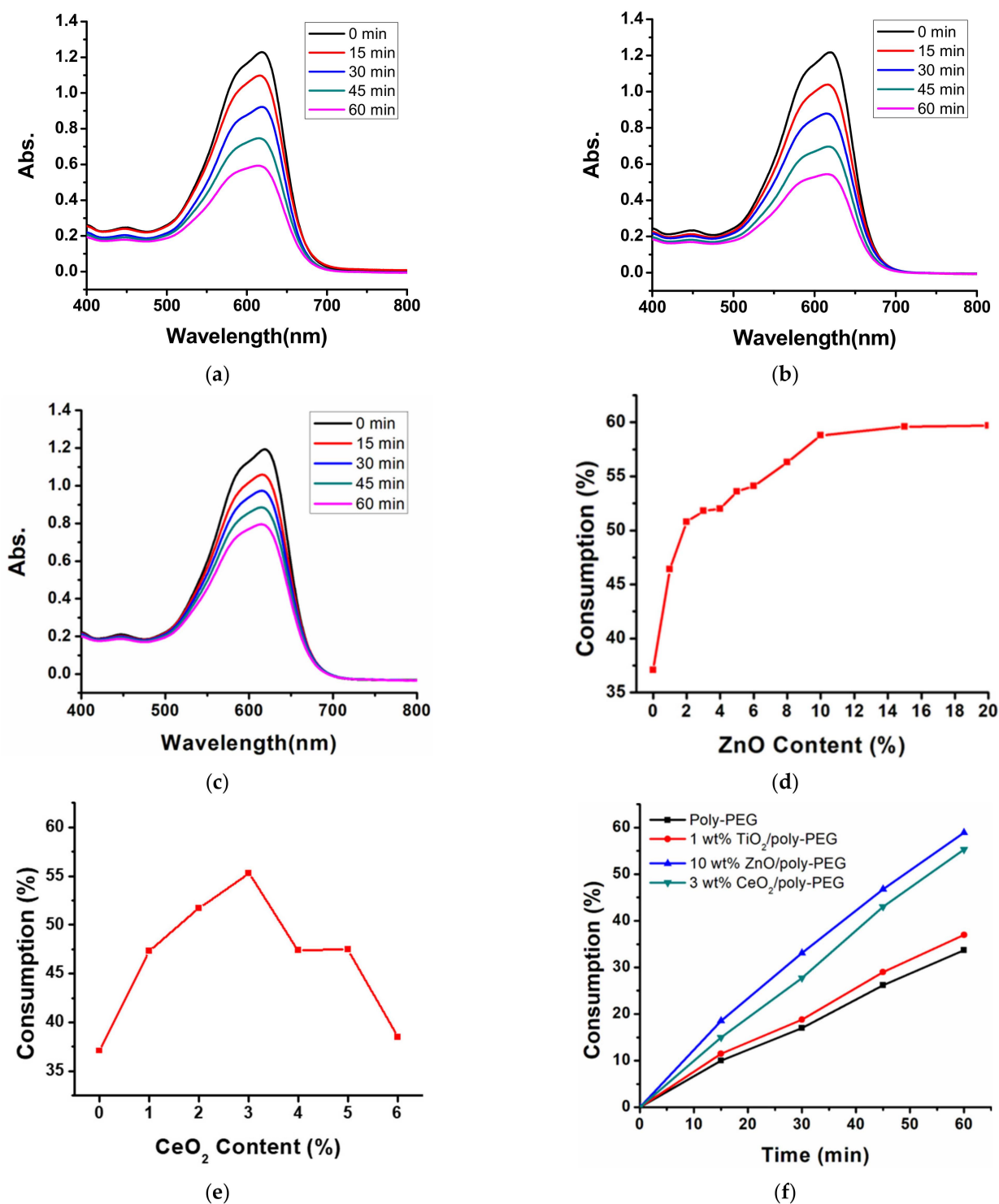
Figure 9. UV–visible absorption spectra of Acid Black (AB) water solutions under air during the photocatalytic degradation process under UV lamp irradiation in the presence of (**a**) 10 wt% ZnO/Poly-PEG composite, (**b**) 3 wt% CeO$_2$/Poly-PEG composite, and (**c**) 1 wt% TiO$_2$/Poly-PEG composite. [AB]$_0$ = 15 ppm, pH = 7. The consumption of Acid Black (15 ppm) with different metal oxide contents under UV lamp irradiation (**d**) in the presence of ZnO/Poly-PEG composite and (**e**) in the presence of CeO$_2$/Poly-PEG composite. Degradation plot of Acid Black (15 ppm) under UV lamp irradiation (**f**) in the presence of Poly-PEG, 1 wt% TiO$_2$/Poly-PEG composite, 10 wt% ZnO/Poly-PEG composite, and 3 wt% CeO$_2$/Poly-PEG composite.

As a common metal oxide photocatalyst, the photocatalytic performance of TiO_2 has been widely known. It has been reported that Acid Black 1 can be degraded by $TPAPP/TiO_2$ under sunlight [43]. As a result, the photocatalytic ability of the new metal oxide/polymer composite was compared with that of TiO_2. The photodegradation properties of 1 wt% TiO_2/Poly-PEG was only about 5% higher than Poly-PEG under the same conditions, but much lower than the samples developed in this research (Figure 9f).

To verify the effect of polymer substrate materials on the catalytic performance of the new photocatalysts, TMPTA was used as an alternative to PEGDA. The experiment under the same conditions of metal oxide/Poly-TMPTA is shown in Figure 10. It can be observed clearly that Poly-TMPTA had no adsorption/swelling capacity for Acid Black aqueous solutions whereas pure Poly-PEG showed significant adsorption (3% vs. 37%). The lack of adsorption capacity seriously affected the overall performance of the composite catalysts. The photocatalytic degradation capacity of 3 wt% CeO_2/Poly-TMPTA for Acid Black was far weaker than that of 3 wt% CeO_2/Poly-PEG. After 15 min of light irradiation, almost no further dye degradation was observed. The lack of swelling of Poly-TMPTA with water severely affected the accessibility of metal oxide particle surfaces by water in the new catalysts. On the contrary, Poly-PEG had the advantage of providing a high-quality and large contact area for the catalyst and reactants, which was extremely beneficial for the catalytic process.
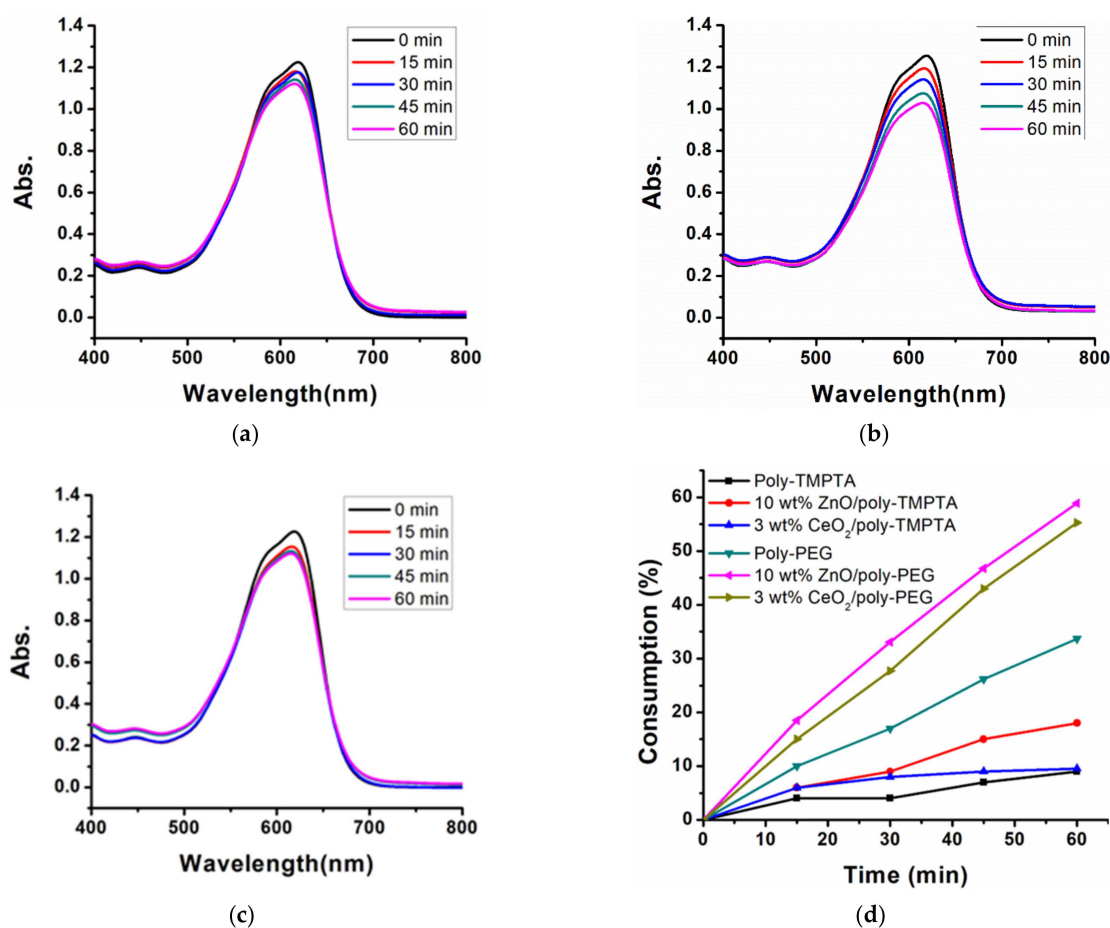

Figure 10. UV–visible absorption spectra of Acid Black water solutions during the photocatalytic degradation process under UV lamp irradiation in the presence of (**a**) Poly-TMPTA, (**b**) 10 wt% ZnO/Poly-TMPTA composite, and (**c**) 3 wt% CeO_2/Poly-TMPTA composite. $[AB]_0$ = 15 ppm, pH = 7. Degradation plot of Acid Black (15 ppm) under Omnicure lamp irradiation (**d**) in the presence of Poly-TMPTA, 10 wt% ZnO/Poly-TMPTA composite, 3 wt% CeO_2/Poly-TMPTA composite, Poly-PEG, 10 wt% ZnO/Poly-PEG, and CeO_2/Poly-PEG composite.

To further determine whether the time of photopolymerization influenced the performance of new photocatalysts, the dye degradation by metal oxide/polymers from syntheses using different irradiation times was investigated and is shown in Figure S1. These curves demonstrated that no significant difference was observed in the catalytic performance of the samples produced at 30 s, 60 s, and 120 s of light irradiation. The consumption of Acid Black was constant for more than one hour of light irradiation, leading to conversions at ~50%. It was clear that 30 s of polymerization (a relatively short time) was sufficient to generate a stable and desirable new catalyst.

The similar dye degradation was studied for another common dye, Eosin-Y (Figure S2). No significant difference in the performance of the samples was observed for the degradation of Eosin-Y, which was rapid and complete. However, it was noteworthy that the performance of Poly-PEG was not significantly different from the other samples, a situation that suggested a dominant role of absorption rather than photocatalysis.

3.5. Metal Oxide/Polymer Composite Recyclability Study

The stability of the photocatalyst is extremely important for practical applications because it meets the requirements of economy, practicality, and environmental protection. So, photocatalytic experiments were repeated three times with the same composite, which was recovered from the dye solution after a depollution cycle, washed several times with water, dried in the open air, and then used again for the next catalytic cycle. As shown in Figure 11, the stability of new photocatalyst was assessed using the cycle tests of 10 wt% ZnO/Poly-PEG composites for Acid Black photodegradation. After the first cycle of dye degradation, the degradation efficiencies began to decline but remained constant for the 2nd cycle and 3rd cycle, demonstrating their high photocatalytic stability by using a simple and low-cost regeneration process.
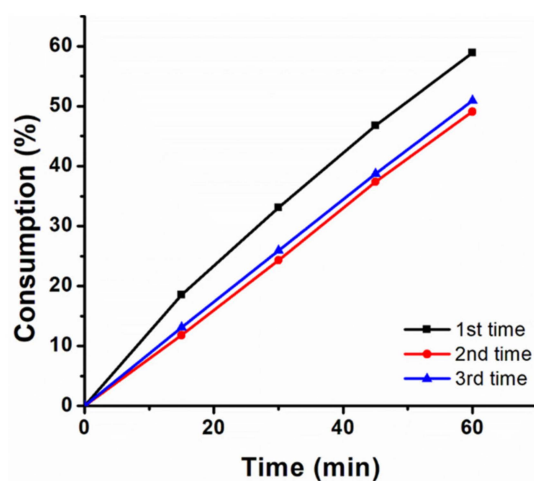

Figure 11. Three consecutive Acid Black photodegradation cycles for 10 wt% ZnO/Poly-PEG composite. $[AB]_0 = 15$ ppm, pH = 7, irradiation source: UV lamp.

3.6. Photocatalytic Degradation Mechanism

The photocatalytic degradation mechanism of ZnO is reported by many researchers (Scheme 2) [44]. The evaluated band gap values are given in Table S1. As a semiconductor photocatalyst, the electrons in the VB band are excited to the CB band of ZnO under the irradiation, leaving holes in the VB band. The O_2 molecules adsorbed on the ZnO surface capture the electrons from the CB band to form superoxide groups ($\cdots O_2^-$), which react with protons in the water ($\cdots O_2H + OH^-$). The surface holes in the VB band react with hydroxyl ions (OH^-) to produce hydroxyl radicals ($\bullet OH$) or are trapped in existing oxygen vacancies. Both $\cdots O_2H$ groups (fragmentation to $\bullet OH$ is likely) and $\bullet OH$ radicals react directly with the organic molecules in the environment to destroy the chromophoric functionality of the model dye. Contaminants in water are in general simpler molecules

such as tensids, mineral oils (aliphatic compounds), etc. Additionally, all organic oxidizable functionalities (-COOH, -OH) will react via photo-Kolbe reaction [23,45] and most will be decomposed/mineralized to CO_2 and water. The •OH have the additional advantage of breaking the unsaturated N=N double bonds by oxidation reaction.
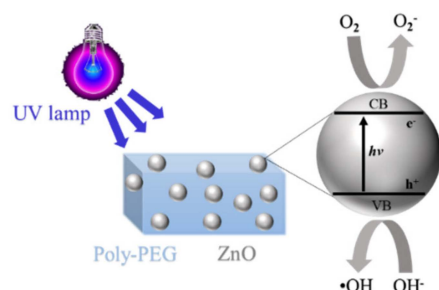
Scheme 2. The mechanism of ZnO/polymer composite photocatalytic reaction. The generated oxygen centered radicals (e.g., •OH) react with the dye to decompose it.

ESR experiments were performed on ZnO/Poly-PEG, before and after photocatalysis, to further investigate the nature of the radicals generated from the reactions on the sample surface. During the Acid Black photodegradation, shown in Figure 12a, a significant decrease occurred in the peak located at g = 1.96 for the ZnO/Poly-PEG. This signal corresponded to a singly ionized oxygen vacancy which was transferred to a double ionized oxygen vacancy ("reaction/generation of hole of the exiton") which did not have an electron and therefore was ESR inactive [46,47]. The regeneration of this signal in the dark could be confirmed. Concerning the photo-Kolbe reaction experiments of ZnO, dispersions were performed and published a few years ago [27].

(a)   (b)
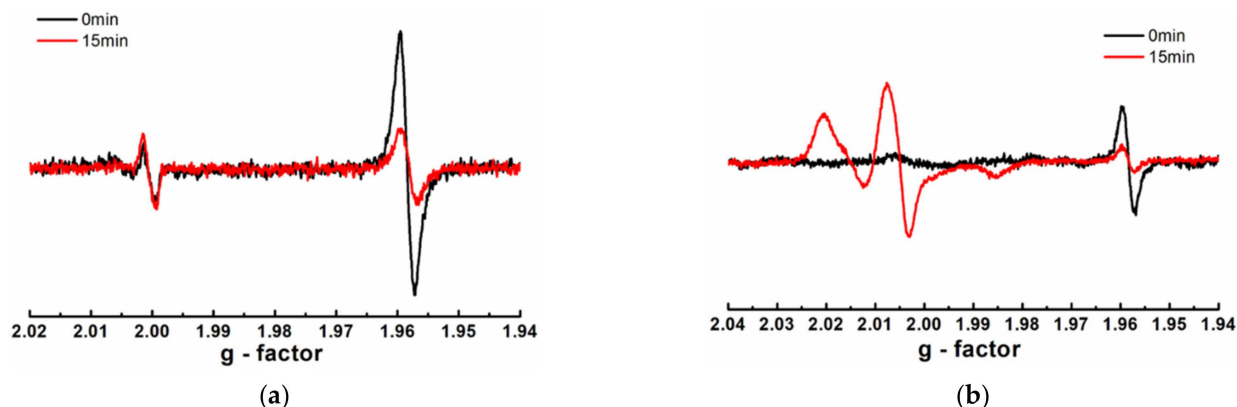
Figure 12. ESR spectra obtained at room temperature (20 °C) from ESR experiments under irradiation with an LED emitting at 405 nm under air. (**a**) ZnO/Poly-PEG, irradiation time = 15 min (**red**) and = 0 min (**black**) spectra, respectively; (**b**) ZnO/Poly-PEG, using PBN = 2 mg/mL (as the spin trap agent), irradiation time = 15 min (**red**) and = 0 min (**black**) spectra.

Additionally, phenyl N-tert-butylnitrone (PBN) was added as a spin trap agent to capture the free radicals produced on the surface ZnO/Poly-PEG during the Acid Black photodegradation reaction. As shown in Figure 12b, located in the range of g = 2.00–2.03, signals were monitored after the reaction, which did not have a symmetric and very well-defined pattern. We assumed that the interaction/adsorption with/on the different surfaces also influenced hyperfine coupling of the unidentifiable nitroxyl-based radicals. It indicated that a reaction led to radicals that can react with solved species.

4. Conclusions

In this paper, metal oxide/polymer composites with enhanced photocatalytic properties, which were synthesized by a simple photopolymerization method, have been demonstrated. In the process of photopolymerization, mild and inexpensive visible LED@405 nm was used as the irradiation source. Curing of one catalytic pellet (8 mm in diameter and 4 mm in height) could be achieved in 30 s. The metal oxide particles in the new composites were successfully incorporated in the polymeric matrix with good stability under conventional conditions. For the photodegradation of Acid Black in aqueous solution, the new metal oxide/polymer composites all showed good performance. The photodegradation efficiency of Acid Black by 10 wt% ZnO/Poly-PEG and 3 wt% CeO_2/Poly-PEG reach 59% and 55% upon 60 min of mercury UV lamp irradiation, respectively. The recyclability of the composites was also demonstrated in the swelling tests and by repeating the degradation measurements with the same sample. After three cycles of photocatalytic reaction, the composites still demonstrated excellent catalytic activity. The previously published and expected reaction mechanism for pure photo-semiconductors was confirmed using the ESR technique for these organic–inorganic composites. The production of free radicals which can be reacted with organic species in the solvent was clearly demonstrated. The approach in this research represents a low-cost and efficient method for the synthesis of reusable composite photocatalysts. It is reasonable to believe that through this approach, polymer-based photocatalysts based on a wider range of species can be used in different applications.

Supplementary Materials: The following supporting information can be downloaded at: https://www.mdpi.com/article/10.3390/photochem2030047/s1, Figure S1: The Acid Black degeneration by 1 wt% ZnO/polymers and 2 wt% ZnO/polymers from syntheses using different irradiation times; Figure S2: UV–visible absorption spectra of Eosin-Y water solutions under air during the photocatalytic degradation process under UV lamp irradiation in the presence of (a) 10 wt% ZnO/Poly-PEG composite. [Eosin-Y]$_0$ = 15 ppm, pH = 7. Degradation plot of Eosin-Y (15 ppm) under Omnicure lamp irradiation (b) in the presence of Poly-PEG, 1 wt% TiO_2/Poly-PEG composite, 10 wt% ZnO/Poly-PEG composite, and 3 wt% CeO_2/Poly-PEG composite; Table S1: The band gap values of composites.

Author Contributions: Conceptualization, J.L., M.S., F.M.-S. and P.X.; synthesis of composites, T.B.; validation, all authors; formal analysis, all authors; data curation, all authors; writing—original draft preparation, all authors; writing—review and editing, all authors. All authors have read and agreed to the published version of the manuscript.

Institutional Review Board Statement: Not applicable.

Informed Consent Statement: Informed consent was obtained from all subjects involved in the study.

Data Availability Statement: Data will be available on request to the authors.

Conflicts of Interest: The authors declare no conflict of interest.

References

1. Chan, S.H.S.; Wu, Y.T.; Juan, J.C.; Teh, C.Y. Recent developments of metal oxide semiconductors as photocatalysts in advanced oxidation processes (AOPs) for treatment of dye waste-water. *J. Chem. Technol. Biotechnol.* **2011**, *86*, 1130–1158. [CrossRef]
2. Raizada, P.; Singh, P.; Kumar, A.; Pare, B.; Jonnalagadda, S.B. Zero valent iron-brick grain nanocomposite for enhanced solar-Fenton removal of malachite green. *Sep. Purif. Technol.* **2014**, *133*, 429–437. [CrossRef]
3. Micheal, K.; Ayeshamariam, A.; Boddula, R.; Arunachalam, P.; AlSalhi, M.S.; Theerthagiri, J.; Prasad, S.; Madhavan, J.; Al-Mayouf, A.M. Assembled composite of hematite iron oxide on sponge-like BiOCl with enhanced photocatalytic activity. *Mater. Sci. Energy Technol.* **2019**, *2*, 104–111. [CrossRef]
4. Sudhaik, A.; Raizada, P.; Shandilya, P.; Singh, P. Magnetically recoverable graphitic carbon nitride and $NiFe_2O_4$ based magnetic photocatalyst for degradation of oxytetracycline antibiotic in simulated wastewater under solar light. *J. Environ. Chem. Eng.* **2018**, *6*, 3874–3883. [CrossRef]

5. Guo, H.-X.; Lin, K.-L.; Zheng, Z.-S.; Xiao, F.-B.; Li, S.-X. Sulfanilic acid-modified P25 TiO$_2$ nanoparticles with improved photocatalytic degradation on Congo red under visible light. *Dye. Pigment.* **2012**, *92*, 1278–1284. [CrossRef]

6. Theerthagiri, J.; Lee, S.J.; Karuppasamy, K.; Arulmani, S.; Veeralakshmi, S.; Ashokkumar, M.; Choi, M.Y. Application of advanced materials in sonophotocatalytic processes for the remediation of environmental pollutants. *J. Hazard. Mater.* **2021**, *412*, 125245. [CrossRef]

7. Naik, S.S.; Lee, S.J.; Theerthagiri, J.; Yu, Y.; Choi, M.Y. Rapid and highly selective electrochemical sensor based on ZnS/Au-decorated f-multi-walled carbon nanotube nanocomposites produced via pulsed laser technique for detection of toxic nitro compounds. *J. Hazard. Mater.* **2021**, *418*, 126269. [CrossRef]

8. Raizada, P.; Sudhaik, A.; Singh, P. Photocatalytic water decontamination using graphene and ZnO coupled photocatalysts: A review. *Mater. Sci. Energy Technol.* **2019**, *2*, 509–525. [CrossRef]

9. Capelo-Martínez, J.L.; Ximénez-Embún, P.; Madrid, Y.; Cámara, C. Advanced oxidation processes for sample treatment in atomic spectrometry. *TrAC Trends Anal. Chem.* **2004**, *23*, 331–340. [CrossRef]

10. Brahmi, C.; Benltifa, M.; Ghali, M.; Dumur, F.; Simonnet-Jégat, C.; Monnier, V.; Morlet-Savary, F.; Bousselmi, L.; Lalevée, J. Polyoxometalates/polymer composites for the photodegradation of bisphenol-A. *J. Appl. Polym. Sci.* **2021**, *138*, 50864. [CrossRef]

11. Ghali, M.; Brahmi, C.; Benltifa, M.; Dumur, F.; Duval, S.; Simonnet-Jégat, C.; Morlet-Savary, F.; Jellali, S.; Bousselmi, L.; Lalevée, J. New hybrid polyoxometalate/polymer composites for photodegradation of eosin dye. *J. Polym. Sci. Part A Polym. Chem.* **2019**, *57*, 1538–1549. [CrossRef]

12. Brahmi, C.; Benltifa, M.; Vaulot, C.; Michelin, L.; Dumur, F.; Millange, F.; Frigoli, M.; Airoudj, A.; Morlet-Savary, F.; Bousselmi, L.; et al. New hybrid MOF/polymer composites for the photodegradation of organic dyes. *Eur. Polym. J.* **2021**, *154*, 110560. [CrossRef]

13. Zhang, R.; Gao, L.; Zhang, Q. Photodegradation of surfactants on the nanosized TiO$_2$ prepared by hydrolysis of the alkoxide titanium. *Chemosphere* **2004**, *54*, 405–411. [CrossRef]

14. Lin, C.; Lin, K.-S. Photocatalytic oxidation of toxic organohalides with TiO$_2$/UV: The effects of humic substances and organic mixtures. *Chemosphere* **2007**, *66*, 1872–1877. [CrossRef] [PubMed]

15. Remucal, C.K. The role of indirect photochemical degradation in the environmental fate of pesticides: A review. *Environ. Sci. Processes Impacts* **2014**, *16*, 628–653. [CrossRef] [PubMed]

16. Bagabas, A.; Alshammari, A.; Aboud, M.F.A.; Kosslick, H. Room-temperature synthesis of zinc oxide nanoparticles in different media and their application in cyanide photodegradation. *Nanoscale Res. Lett.* **2013**, *8*, 516. [CrossRef]

17. Grabowska, E.; Reszczyńska, J.; Zaleska, A. RETRACTED: Mechanism of phenol photodegradation in the presence of pure and modified-TiO$_2$: A review. *Water Res.* **2012**, *46*, 5453–5471. [CrossRef]

18. Dasary, S.S.R.; Saloni, J.; Fletcher, A.; Anjaneyulu, Y.; Yu, H. Photodegradation of Selected PCBs in the Presence of Nano-TiO$_2$ as Catalyst and H$_2$O$_2$ as an Oxidant. *Int. J. Environ. Res. Public Health* **2010**, *7*, 3987–4001. [CrossRef]

19. Wu, X.; Shao, Y. Study of Kinetics Mechanism of PAHs Photodegradation in Solution. *Procedia Earth Planet. Sci.* **2017**, *17*, 348–351. [CrossRef]

20. Priya, B.; Shandilya, P.; Raizada, P.; Thakur, P.; Singh, N.; Singh, P. Photocatalytic mineralization and degradation kinetics of ampicillin and oxytetracycline antibiotics using graphene sand composite and chitosan supported BiOCl. *J. Mol. Catal. A Chem.* **2016**, *423*, 400–413. [CrossRef]

21. Sudhaik, A.; Raizada, P.; Shandilya, P.; Jeong, D.-Y.; Lim, J.-H.; Singh, P. Review on fabrication of graphitic carbon nitride based efficient nanocomposites for photodegradation of aqueous phase organic pollutants. *J. Ind. Eng. Chem.* **2018**, *67*, 28–51. [CrossRef]

22. Schmitt, M.; Becker, D.; Lalevée, J. Performance analysis of the solidification of acrylic esters photo-initiated by systematically modified ZnO nanoparticles. *Polymer* **2018**, *158*, 83–89. [CrossRef]

23. Schmitt, M. Synthesis and testing of ZnO nanoparticles for photo-initiation: Experimental observation of two different non-migration initiators for bulk polymerization. *Nanoscale* **2015**, *7*, 9532–9544. [CrossRef] [PubMed]

24. Schmitt, M.; Lalevée, J. ZnO nanoparticles as polymerisation photo-initiator: Levulinic acid/NaOH content variation. *Colloids Surf. A Physicochem. Eng. Asp.* **2017**, *532*, 189–194. [CrossRef]

25. Chelli, V.R.; Golder, A.K. Ag-doping on ZnO support mediated by bio-analytes rich in ascorbic acid for photocatalytic degradation of dipyrone drug. *Chemosphere* **2018**, *208*, 149–158. [CrossRef] [PubMed]

26. Wang, Z.; Liu, S.; Zhang, J.; Yan, J.; Zhao, Y.; Mahoney, C.; Ferebee, R.; Luo, D.; Pietrasik, J.; Bockstaller, M.R.; et al. Photocatalytic Active Mesoporous Carbon/ZnO Hybrid Materials from Block Copolymer Tethered ZnO Nanocrystals. *Langmuir* **2017**, *33*, 12276–12284. [CrossRef]

27. Schmitt, M.; Kuhn, S.; Wotocek, M.; Hempelmann, R. Photo-Curing of off-set Printing Inks by Functionalized ZnO Nanoparticles. *Z. Für Phys. Chem.* **2011**, *225*, 297–311. [CrossRef]

28. Schmitt, M.; Garra, P.; Lalevée, J. Bulk Polymerization Photo-Initiator ZnO: Increasing of the Benzoyl Formic Acid Concentration and LED Illumination. *Macromol. Chem. Phys.* **2018**, *219*, 1800208. [CrossRef]

29. Schmitt, M.; Dietlin, C.; Lalevée, J. Towards Visible LED Illumination: ZnO-ZnS Nanocomposite Particles. *ChemistrySelect* **2020**, *5*, 985–987. [CrossRef]

30. Sahoo, G.P.; Samanta, S.; Bhui, D.K.; Pyne, S.; Maity, A.; Misra, A. Hydrothermal synthesis of hexagonal ZnO microstructures in HPMC polymer matrix and their catalytic activities. *J. Mol. Liq.* **2015**, *212*, 665–670. [CrossRef]

31. Qiu, R.; Zhang, D.; Mo, Y.; Song, L.; Brewer, E.; Huang, X.; Xiong, Y. Photocatalytic activity of polymer-modified ZnO under visible light irradiation. *J. Hazard. Mater.* **2008**, *156*, 80–85. [CrossRef] [PubMed]

32. Rezaei, S.J.T.; Nabid, M.R.; Hosseini, S.Z.; Abedi, M. Polyaniline-Supported Zinc Oxide (ZnO) Nanoparticles: An Active and Stable Heterogeneous Catalyst for the Friedel–Crafts Acylation Reaction. *Synth. Commun.* **2012**, *42*, 1432–1444. [CrossRef]

33. Vidya, C.; Manjunatha, C.; Chandraprabha, M.N.; Rajshekar, M.; Mal, A.R. Hazard free green synthesis of ZnO nano-photo-catalyst using Artocarpus Heterophyllus leaf extract for the degradation of Congo red dye in water treatment applications. *J. Environ. Chem. Eng.* **2017**, *5*, 3172–3180. [CrossRef]

34. Kurian, M.; Kunjachan, C. $Ce_xV_{1-x}O_2$ (x: 0, 0.25–1) nanocomposites as efficient catalysts for degradation of 2,4 dichlorophenol. *J. Environ. Chem. Eng.* **2016**, *4*, 1359–1366. [CrossRef]

35. López-Tenllado, F.J.; Murcia-López, S.; Gómez, D.M.; Marinas, A.; Marinas, J.M.; Urbano, F.J.; Navío, J.A.; Hidalgo, M.C.; Gatica, J.M. A comparative study of Bi_2WO_6, CeO_2, and TiO_2 as catalysts for selective photo-oxidation of alcohols to carbonyl compounds. *Appl. Catal. A Gen.* **2015**, *505*, 375–381. [CrossRef]

36. Issarapanacheewin, S.; Wetchakun, K.; Phanichphant, S.; Kangwansupamonkon, W.; Wetchakun, N. Efficient photocatalytic degradation of Rhodamine B by a novel CeO_2/Bi_2WO_6 composite film. *Catal. Today* **2016**, *278*, 280–290. [CrossRef]

37. Craciun, R.; Daniell, W.; Knözinger, H. The effect of CeO_2 structure on the activity of supported Pd catalysts used for methane steam reforming. *Appl. Catal. A Gen.* **2002**, *230*, 153–168. [CrossRef]

38. Liang, M.; Borjigin, T.; Zhang, Y.; Liu, B.; Liu, H.; Guo, H. Controlled assemble of hollow heterostructured $g-C_3N_4@CeO_2$ with rich oxygen vacancies for enhanced photocatalytic CO_2 reduction. *Appl. Catal. B Environ.* **2019**, *243*, 566–575. [CrossRef]

39. Ma, W.; Mashimo, T.; Tamura, S.; Tokuda, M.; Yoda, S.; Tsushida, M.; Koinuma, M.; Kubota, A.; Isobe, H.; Yoshiasa, A. Cerium oxide (CeO_{2-x}) nanoparticles with high Ce^{3+} proportion synthesized by pulsed plasma in liquid. *Ceram. Int.* **2020**, *46*, 26502–26510. [CrossRef]

40. Khan, M.M.; Ansari, S.A.; Pradhan, D.; Han, D.H.; Lee, J.; Cho, M.H. Defect-Induced Band Gap Narrowed CeO_2 Nanostructures for Visible Light Activities. *Ind. Eng. Chem. Res.* **2014**, *53*, 9754–9763. [CrossRef]

41. Wu, J.; Wang, J.; Du, Y.; Li, H.; Yang, Y.; Jia, X. Chemically controlled growth of porous CeO_2 nanotubes for Cr(VI) photoreduction. *Appl. Catal. B Environ.* **2015**, *174–175*, 435–444. [CrossRef]

42. Shcherbakov, A.B.; Reukov, V.V.; Yakimansky, A.V.; Krasnopeeva, E.L.; Ivanova, O.S.; Popov, A.L.; Ivanov, V.K. CeO_2 Nanoparticle-Containing Polymers for Biomedical Applications: A Review. *Polymers* **2021**, *13*, 924. [CrossRef] [PubMed]

43. Krishnakumar, B.; Balakrishna, A.; Arranja, C.T.; Dias, C.M.F.; Sobral, A.J.F.N. Chemically modified amino porphyrin/TiO_2 for the degradation of Acid Black 1 under day light illumination. *Spectrochim. Acta Part A Mol. Biomol. Spectrosc.* **2017**, *176*, 134–141. [CrossRef] [PubMed]

44. Gu, X.; Li, C.; Yuan, S.; Ma, M.; Qiang, Y.; Zhu, J. ZnO based heterojunctions and their application in environmental photocatalysis. *Nanotechnology* **2016**, *27*, 402001. [CrossRef] [PubMed]

45. Schmitt, M. ZnO Nanoparticle Induced Photo-Kolbe Reaction, Fragment Stabilization and Effect on Photopolymerization Monitored by Raman–UV-Vis Measurements. *Macromol. Chem. Phys.* **2012**, *213*, 1953–1962. [CrossRef]

46. Schmitt, M. *UV-Härtung von Acrylsäureestern Durch Nanoskalige Metalloxide*; Suedwestdeutscher Verlag fuer Hochschulschriften: Saarbrücken, Germany, 2009.

47. Gurylev, V.; Perng, T.P. Defect engineering of ZnO: Review on oxygen and zinc vacancies. *J. Eur. Ceram. Soc.* **2021**, *41*, 4977–4996. [CrossRef]